Nonlinear susceptibilities as a probe to unambiguously distinguish between canonical and cluster spin glasses

Yugandhar Bitla and S. N. Kaul*
School of Physics, University of Hyderabad, Central University P. O., Hyderabad 500 046, Andhra Pradesh, India

L. Fernández Barquín
Departamento CITIMAC, Universidad de Cantabria, E-39005 Santander, Spain

(Received 5 October 2011; revised manuscript received 11 December 2011; published 4 September 2012)

Treating the randomly Fe-substituted optimally hole-doped manganite $La_{0.7}Pb_{0.3}(Mn_{1-y}Fe_y)O_3$ ($y = 0.2,0.3$) as a test case, we demonstrate that a combined investigation of both odd and even harmonics of the ac magnetic response permits an unambiguous distinction between the canonical and cluster spin glasses. As expected for a spin glass (SG), the nonlinear ac magnetic susceptibilities $\chi_3(T,\omega)$ and $\chi_5(T,\omega)$ (odd harmonics) diverge at the SG freezing temperature $T_g = 80.00(3)$ K [$T_g = 56.25(5)$ K] in the static limit and, like the imaginary part of the linear susceptibility, follow dynamic scaling with the critical exponents $\beta = 0.56(3)$ [$\beta = 0.63(3)$], $\gamma = 1.80(5)$ [$\gamma = 2.0(1)$], and $z\nu = 10.1(1)$ [$z\nu = 8.0(5)$] in the sample with composition $y = 0.2$ ($y = 0.3$). The nonlinear susceptibility χ_{NL}, which has contributions from both χ_3 and χ_5, satisfies static scaling with the same choice of T_g, β, and γ. Irrespective of the Fe concentration, the values of the critical exponents γ, ν, and η are in much better agreement with those theoretically predicted for a three-dimensional ($d = 3$) Heisenberg chiral SG than for a $d = 3$ Ising SG. The true thermodynamic nature of the "zero-field" spin-glass transition is preserved even in finite magnetic fields. Unlike odd harmonics, even harmonics $\chi_2(T,\omega)$ and $\chi_4(T,\omega)$ make it evident that, apart from the macroscopic length scale of the spin-glass order in the static limit, there exists a length scale that corresponds to the short-range ferromagnetic order.

DOI: 10.1103/PhysRevB.86.094405 PACS number(s): 75.40.Gb, 75.40.Cx, 75.50.Lk, 75.47.Lx

I. INTRODUCTION

It is well-known[1] that the spin-glass (SG) state at temperatures below the spin-freezing temperature T_g is characterized by an extremely slow (logarithmic) spin dynamics, aging and memory effects, bifurcation in the "zero-field-cooled" (ZFC) and "field-cooled" (FC) thermomagnetic curves at low fields, and a divergence in the nonlinear susceptibility at T_g. These characteristic properties of SG behavior have been observed in a wide variety of systems ranging from the so-called canonical spin glasses[2] [dilute magnetic alloys such as Au(Fe), Cu(Mn), or Ag(Mn) with mostly individual spins and a sparse population of minute spin clusters cooperatively participating in the spin-freezing process] to cluster spin glasses or mictomagnets[1] [magnetic alloys with concentration close to the percolation threshold for the onset of long-range ferromagnetic (FM) or antiferromagnetic (AFM) ordering and a strong tendency to form interacting spin clusters of assorted size]. Thus, the above experimental signatures, on their own, fail to make a clear-cut distinction between a canonical SG and a cluster SG. The standard theoretical description of spin glasses considers Heisenberg interactions with random exchange coupling between the (magnetic impurity) spins in the presence or absence of a weak Ising anisotropy and thereby leads to $d = 3$ (d is the space dimension) Ising or Heisenberg universality classes. In the latter case, the SG transition occurs at a finite T_g only when either dipolar (anisotropic) interactions are included[3] or a weak coupling exists between the spin and chirality (a multispin variable describing the left- or right-handedness of the noncollinear or noncoplanar spin structures induced by frustration) sectors.[4–7] Therefore, for a meaningful comparison between theory and experiment, the spin structure at microscopic length scales (i.e., collinear FM or AFM or noncollinear spin order within the clusters or correlated local regions) must be known *a priori*.

In this paper, we demonstrate how the nonlinear (NL) magnetic susceptibilities unambiguously distinguish between a cluster SG and a canonical SG, and directly probe the magnetic order (FM or AFM) prevalent within the clusters. To this end, we treat the randomly Fe-substituted optimally hole-doped manganite $La_{0.7}Pb_{0.3}(Mn_{1-y}Fe_y)O_3$ ($y = 0.2,0.3$) as a test case. The rationale behind the choice of this system is as follows. First, nanoscale phase separation, and hence the formation of spin-correlated regions or spin clusters, is well documented[8] in manganites. Second, the nature of magnetic order in this manganite system for $y \geqslant 0.2$ is highly controversial.[9–15] On the one hand, spin-polarized neutron diffraction[12,13,15] (SPND), small-angle neutron scattering[13] (SANS), muon spin relaxation[12] (μSR), and neutron spin-echo[14] (NSE) experiments strongly indicate that, as y increases, the AFM superexchange interactions grow at the expense of FM double-exchange interactions so that the FM correlated regions shrink in size to the extent that the long-range FM order ceases to exist for $y \geqslant 0.2$. On the other hand, based on bulk magnetization measurements[10,11] mainly, it is claimed[11] that the long-range FM order is present even up to Fe concentrations as high as $y = 0.4$ and beyond this concentration, a long-range AFM order sets in. These controversies are put to rest by providing conclusive evidence for a cluster spin-glass state in the compositions $y = 0.2$ and $y = 0.3$.

II. EXPERIMENTAL DETAILS

The $La_{0.7}Pb_{0.3}(Mn_{1-y}Fe_y)O_3$ samples with $y = 0.2$ and $y = 0.3$ were prepared in the nanocrystalline (average grain

size $\simeq 100$ nm) form by the sol-gel method and are the same as those used previously for the SPND, SANS, μSR, and NSE experiments.[12–15] Magnetic susceptibility at a static magnetic field of $H \equiv H_{dc} = 10$ Oe, $\chi_{dc}(H = 10\ \text{Oe})$, was recorded over the temperature range $2 \leqslant T \leqslant 300$ K in both the ZFC and FC modes. The bifurcation, marking the onset of magnetic irreversibility, in the ZFC and FC $\chi_{dc}(T, H = 10\,\text{Oe})$ curves opens up at $T < T_{\text{irr}} = 80$ K. The first five harmonics of the ac magnetic response, $\chi_n(\omega,T,H) = \chi_n'(\omega,T,H) + i\chi_n''(\omega,T,H)$ with $n = 1,2,3,4,5$, were measured at 0.5, 0.2, 0.1, 0.2, and 0.5 K steps in the temperature ranges 2–10 K, 10–60 K, 60–100 K, 100–120 K, and 120–150 K, respectively, at the rms amplitudes $h = 0.1,1,5,10$ Oe and frequencies $10\ \text{Hz} \leqslant \omega \leqslant 10$ kHz of the ac driving field in the absence or presence of static fields in the range $30\ \text{Oe} \leqslant H \leqslant 1$ kOe. In these measurements, dc and/or ac fields were applied after a fixed waiting time t_w of 5 min. After identifying the spin-glass transition temperature T_g with the *frequency-independent* temperature where the nonlinear susceptibilities $\chi_3(T)$ and $\chi_5(T)$ peak, i.e., $T_g = 80$ K, in the next experimental run, the dependence of $\chi_n(\omega,T,H)$ on the waiting time was recorded up to $t_w = 30$ min ($t_w = 15$ min) at fixed temperatures in steps of <100 mK (0.2 K) over the temperature range $78 \leqslant T \leqslant 82$ K (down to 60 K and up to 100 K, outside this range). We could not carry out experiments at frequencies lower than 10 Hz for very long times since the accessible frequency window for high-precision measurements on the Quantum Design physical property measurement system–AC measurement system-magnetometer is limited to the frequency range 10 Hz–10 kHz. Since the samples with Fe concentrations $y = 0.2$ and $y = 0.3$ yield essentially similar results, the χ_n ($n = 1$–5) data for $y = 0.2$ only are presented here and the final results for $y = 0.3$ are quoted at the end. Unless specified otherwise, $\chi_n = \chi_n'$ since $\chi_n' \gg \chi_n''$.

III. RESULTS AND DISCUSSION

Figure 1 shows that, as a function of temperature, the linear susceptibility χ_1 goes through a broad peak, centered at $T_p \simeq 80$ K, which is reduced slightly in height and shifts to *higher* temperatures with increasing ac driving-field frequency ω. By contrast, this peak gets greatly suppressed, smeared out, and displaced to *lower* temperatures as the superposed dc magnetic field H increases in strength. The observation that T_p depends on *frequency* precludes the possibility of a true thermodynamic FM-to-PM (paramagnetic) phase transition at T_p but instead reflects the nonergodic behavior normally associated with spin glasses. If the peak temperature T_p is identified with the spin-glass freezing temperature T_g, the relative variation in T_g per decade of frequency, $\Delta T_g/\{T_g \Delta(\log_{10}\omega)\}$, is $3.1(2) \times 10^{-2}$ [$2.0(2) \times 10^{-2}$] for $y = 0.2$ [$y = 0.3$]. These values compare favourably with $\simeq 6 \times 10^{-2}$ or $\simeq 2 \times 10^{-2}$ reported previously for the insulating[1] (Eu,Sr)S or semiconducting[16] $Cd_{0.6}Mn_{0.4}Te$ and[17] $Zn_{0.1}Mn_{0.9}In_2Te_4$ spin glasses but are an order of magnitude greater than $\simeq 5 \times 10^{-3}$ observed[1] in CuMn and AuMn metallic canonical spin glasses. This finding is consistent with the insulating or semiconducting behavior[9,12] of the samples with $y = 0.2$ and $y = 0.3$ down to 2 K. Another important observation is that the peak at T_p is *much broader* and $\chi_1(T)$ is *two orders of magnitude larger* than that in the canonical spin glasses.[2] A broad peak at T_p and a huge enhancement in $\chi_1(T)$ are indicative of the presence of FM clusters.

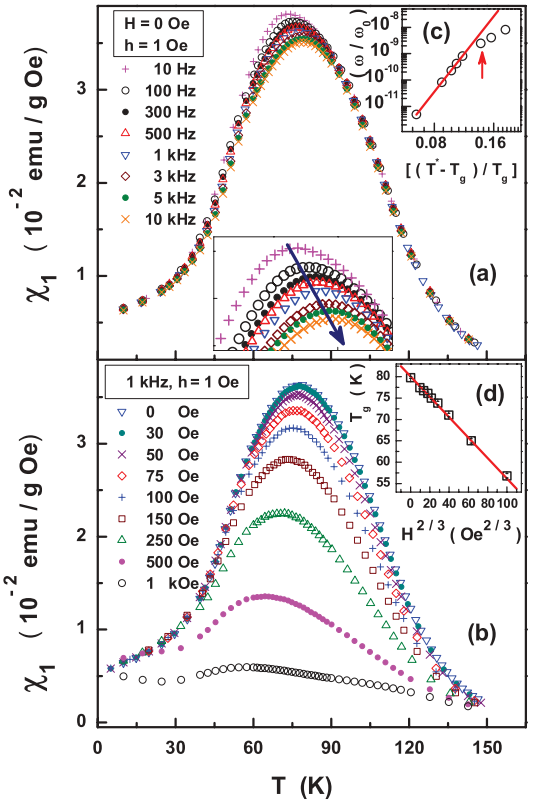

FIG. 1. (Color online) The variations of the linear susceptibility χ_1 with temperature (a) at different frequencies when $H = 0$ Oe and $h = 1$ Oe [the enlarged view of the peak in $\chi_1(T)$ serves to highlight the shift in the peak with frequency], and (b) at different static fields H when $h = 1$ Oe and $\omega = 1$ kHz. The inset (c) of (a) testifies to the validity of the critical-slowing-down model, Eq. (1), in the static limit, by demonstrating that the plot of $\log_{10}(\omega/\omega_0)$ versus $\log_{10}\{[T^*(\omega) - T_g]/T_g\}$ is *linear* for frequencies $\omega \leqslant 1$ kHz [the upward arrow marks the onset of strong deviations from Eq. (1) at $\omega = 3$ kHz] while the inset (d) of (b) shows that the spin-glass temperature T_g has the same dependence on the static field H as the Almeida-Thouless irreversibility line in the (T,H) plane of a $d = 3$ Ising spin glass or as the spin-glass phase transition line at low fields within the chiral scenario of a $d = 3$ Heisenberg spin glass with weak random magnetic anisotropy.

A. Critical slowing down

In the case of a continuous second-order phase transition, the spin-spin correlation length (ξ) diverges as $\xi \sim \epsilon^{-\nu}$ [where the reduced temperature $\epsilon = (T - T_g)/T_g$ and ν is the static critical exponent] when T_g is approached from above. Assuming the conventional critical slowing down on approaching T_g from high temperatures, the relaxation time ($\tau = 2\pi/\omega$) due to the correlated dynamics is related to ξ as $\tau \propto \xi^z$, where z is the dynamic critical exponent. This relation for τ, when recast in terms of the measurement frequency ω, yields

$$\omega = \omega_0 \left[\frac{T^*(\omega) - T_g}{T_g}\right]^{z\nu}. \qquad (1)$$

If $T^*(\omega) = T_p(\omega)$, Eq. (1) is approximately followed over the entire frequency range with the values $\tau_0 = 2\pi/\omega_0 = 1.25(50) \times 10^{-12}$ s, $z\nu = 10.0(10)$, and $T_g = 70.0(10)$ K. This approach yields a much lower value of T_g than that obtained from the scaling analysis of the nonlinear susceptibilities in Sec. III B. This is so because such an assignment defines a set of $T^*(\omega)$ values for which τ is not necessarily constant, as should be the case for Eq. (1) to be applicable. To remedy this, we use the criterion[18] that $T^*(\omega)$ is the temperature at which the quantity $\tan\theta = \chi''/\chi' = \omega\tau_{\rm av}$ is a constant. This is true only when the phase angle θ is so small (e.g., $\lesssim 0.1^\circ$) that $\tan\theta \approx \theta = $ const. At a given frequency, T^* thus marks the temperature at which $\theta(T)$ goes through a minimum ($\sim 0.05^\circ$). In accordance with Eq. (1), the plot of $\log_{10}(\omega/\omega_0)$ versus $\log_{10}\{[T^*(\omega) - T_g]/T_g\}$, shown in the inset (c) of Fig. 1(a), is linear for frequencies $\omega \leqslant 1$ kHz with the choice of parameters $\tau_0 = 5.2(6) \times 10^{-12}$ s, $z\nu = 9.5(8)$, and $T_g = 79.9(4)$ K. The values of $z\nu$ and T_g so obtained agree quite well with those determined from the static (dynamic) scaling of χ_{nl} (χ_3 and χ_5) in Sec. III B. However, the deviations from Eq. (1) progressively grow as the driving field frequency increases beyond 3 kHz. The source of these deviations is addressed in Sec. III E.

B. Static and dynamic scaling of nonlinear susceptibilities

In the static limit ($\omega \to 0$), magnetization of a spin-glass system, at temperatures below or above T_g, can be expressed in the powers of the applied dc magnetic field H as

$$M = \chi_1 H + \chi_3 H^3 + \chi_5 H^5 + \cdots . \tag{2}$$

The terms with even powers of H do not appear in the above expression for the following reason. The even harmonics in the magnetic response, i.e., the NL susceptibilities $\chi_2, \chi_4, \ldots$ are zero[19] for an ideal SG at temperatures $T \gtrless T_g$ because they are proportional to the spontaneous magnetization M_0 or its powers, and $M_0 = 0$ in both SG and PM phases. By contrast, for a ferromagnet, χ_2 and χ_4 are (finite) *negative*, *diverge* as T_c is approached from below, and, in the mean-field description,[20] abruptly jump to zero at $T = T_c$ and stay at zero for $T > T_c$. If the SG-PM phase transition occurs at a finite temperature T_g, χ_1 is *nonsingular* but the NL susceptibilities $\chi_3, \chi_5, \ldots$ diverge[19,21] at $T = T_g$. Again, in sharp contrast with this behavior, in a ferromagnet, χ_1 and χ_5 are positive and diverge at $T = T_c$ whereas χ_3 is positive, changes sign at $T = T_c$, and diverges on both sides of T_c.[20] Thus, based on the temperature variations of χ_n ($n = 1$–5), a spin glass can be unambiguously distinguished from a ferromagnet, or even from an antiferromagnet.[19]

The NL susceptibility $\chi_{\rm nl}$ at a static field H defined as $\chi_{\rm nl} = (M/H) - \chi_1 = \chi_3 H^2 + \chi_5 H^4 + \cdots$, can, in the vicinity of $T = T_g$, be expressed as a function of a single variable $H^2/\epsilon^{\beta+\gamma}$ as[2]

$$\chi_{\rm nl} = \epsilon^{\beta}\, G(H^2/\epsilon^{\beta+\gamma}), \tag{3}$$

where $G(x)$ is the static scaling function while β and γ are the critical exponents for the SG order parameter and χ_3, respectively. The critical exponents γ and $\beta + 2\gamma$ characterize the divergence[2] of χ_3 and χ_5, respectively, as T_g is approached from above. When, instead of a static field, a time-varying field $H(t) = H + h\sin\omega t$ with $h/H \ll 1$ is applied, the NL susceptibility is given by the expression[2,22] $\chi'_{\rm nl} = (\partial m/\partial h) - \chi_1 = 3\chi_3 H^2 + 5\chi_5 H^4 + \cdots$, where m is the ac component of magnetization. The frequency-dependent NL susceptibilities $\chi_3(\epsilon,\omega)$ and $\chi_5(\epsilon,\omega)$, in the above expression for $\chi'_{\rm nl}$, follow the dynamic scaling equations of state[2]

$$\chi_n(\epsilon,\omega)/\epsilon^{-\gamma_n} = g_n(\omega/\epsilon^{z\nu}) \tag{4}$$

with $n = 3,5, \ldots$, $g_n(x)$ the corresponding dynamic scaling function, $\gamma_3 = \gamma$, and $\gamma_5 = \beta + 2\gamma$.

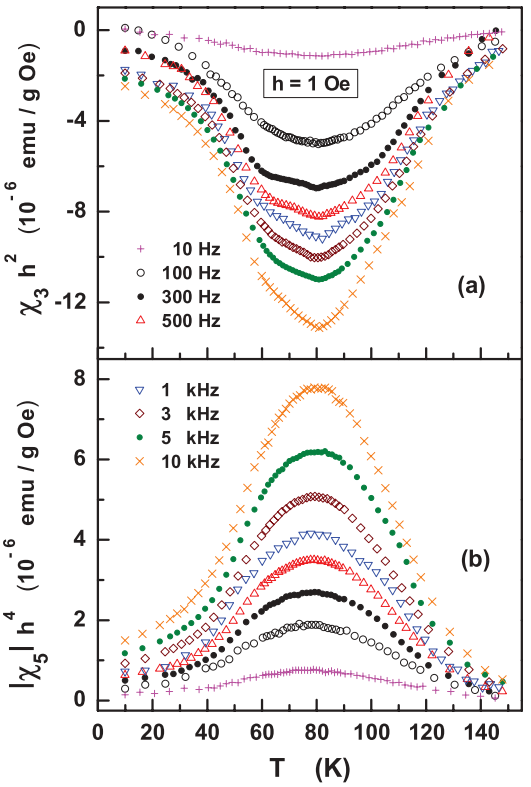

FIG. 2. (Color online) Temperature variations of the nonlinear susceptibilities (a) χ_3 and (b) χ_5 at various fixed frequencies when $H = 0$ Oe and $h = 1$ Oe.

While the divergence of χ_3 at $T = T_g$ together with the static scaling, Eq. (3), and dynamic scaling, Eq. (4), of the NL susceptibility constitute a stringent test for ascertaining whether or not a spin-glass state exists and a phase transition to the PM state occurs at a finite temperature $T = T_g$, the critical exponents β, γ, and $z\nu$ decide the universality class ($d = 3$ Ising or Heisenberg SG) to which a given system belongs.

Unlike T_p in $\chi_1(T)$, the temperature $T_p^{\rm nl} = 80$ K, at which the $|\chi_3(T)|$ and $|\chi_5(T)|$ curves (taken at fixed frequencies) peak, *does not depend on the frequency* of the ac driving field, as should be the case for a true thermodynamic phase transition. This conclusion rests on the observation that no shift in $T_p^{\rm nl}$ with ω over three decades of frequency [Figs. 2(a) and 2(b)] could be discerned within the measurement temperature interval of $\simeq 30$ mK around $T_p^{\rm nl}$. To determine the true asymptotic value of the exponent γ, we make use of the "range-of-fit" (ROF) data analysis, detailed in Ref. 23, and the following expression for $\chi_3(T)$:

$$\begin{aligned}\chi_3^{-1}(T) &= \left[\chi_3^{\rm int}(T)\right]^{-1} + \text{const} \\ &= A_{\rm eff}(T)\,\epsilon^{\gamma_{\rm eff}(T)} + \text{const} \quad (\epsilon > 0),\end{aligned} \tag{5}$$

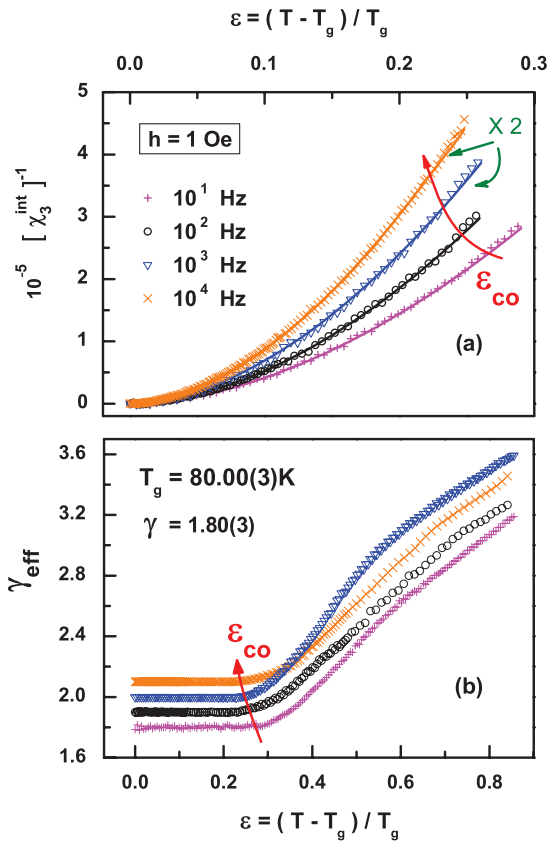

FIG. 3. (Color online) (a) $[\chi_3^{\rm int}]^{-1}(\epsilon)$ (symbols), in a temperature range wider than the asymptotic critical region (ACR) ($\epsilon \leqslant \epsilon_{co}$), at the ac driving field frequencies $\omega = 10^1, 10^2, 10^3, 10^4$ Hz and amplitude $h = 1$ Oe, along with the theoretical fits (continuous curves), based on Eq. (5) of the text, obtained in the ACR. Note that the $[\chi_3^{\rm int}]^{-1}(\epsilon)$ data corresponding to $\omega = 10^3$ and 10^4 Hz are multiplied by a factor of 2, in (a). (b) The temperature variations of the effective critical exponent for χ_3 yielded by the range-of-fit analysis based on Eq. (5). For the sake of clarity, the $\gamma_{\rm eff}(\epsilon)$ data for $\omega = 10^2, 10^3$, and 10^4 Hz are shifted up by 0.1, 0.2, and 0.3, respectively, with respect to that for $\omega = 10^1$ Hz.

where $\chi_3^{\rm int}$ is the intrinsic nonlinear (third harmonic or second-order) susceptibility that diverges at T_g, and the effective critical exponent for χ_3, $\gamma_{\rm eff}$, depends on temperature and attains the constant limiting value γ in the asymptotic critical region (ACR), i.e., $\gamma_{\rm eff}(\epsilon) \to \gamma$ as $\epsilon \to 0$. The constant in Eq. (5) accounts for the fact that the finite size of the system limits the divergence of χ_3 at $\epsilon = 0$ (i.e., at $T = T_g$). As an illustration, Fig. 3(a) shows the theoretical fits to $[\chi_3^{\rm int}(T)]^{-1}$ $[= \chi_3^{-1}(T) - \chi_3^{-1}(T = T_g)]$ at $\omega = 10^1, 10^2, 10^3, 10^4$ Hz, $h = 1$ Oe, and $H = 0$, based on Eq. (5) with $\gamma_{\rm eff} = 1.80$, obtained in the ACR. The $[\chi_3^{\rm int}(T)]^{-1}$ data deviate from such fits (continuous curves) when the temperature exceeds the crossover temperature ϵ_{co}, which marks the upper bound of the ACR. The width of the ACR shrinks with increasing frequency as ϵ_{co} reduces from 0.27 at $\omega = 10^1$ Hz to 0.23 at $\omega = 10^4$ Hz. The ROF analysis yields $T_g = 80.00(3)$ K, $\gamma_{\rm eff}(\epsilon)$ [as depicted in Fig. 3(b)] and the *frequency-independent* value $\gamma = 1.80(3)$ in the ACR, which extends over the range $1.0 \times 10^{-3} \leqslant \epsilon \lesssim 2.5 \times 10^{-1}$ for $10^1 \leqslant \omega \leqslant 10^4$ Hz. By following the same procedure as above for analyzing the $\chi_5(T)$ data, we arrive at the value 4.16(6) for the exponent $\beta + 2\gamma$, implying thereby that the exponent $\beta = 0.56(2)$. Note that the $\chi_3(T)$ and $\chi_5(T)$ data taken at $h = 0.1$ Oe over the frequency range $10^1 \leqslant \omega \leqslant 10^4$ Hz yield exactly the same values for the critical exponents β and γ as those for $h = 1$ Oe. The frequency-independent values for the critical exponents strongly indicate that the *static* critical exponents have been determined in this work.

That the true thermodynamic nature of the zero-field spin-glass transition is *preserved even in finite magnetic fields* is corroborated by the observation that the well-defined $T_g(H)$, marking the temperature at which the $|\chi_3(T)|_{\omega,H}$ or $|\chi_5(T)|_{\omega,H}$ curves peak, is independent of ω over three decades of frequency and decreases with increasing H, as shown in the inset (d) of Fig. 1(b) at a representative frequency of 10^3 Hz.

In order to verify if the static scaling, Eq. (3), holds in the present case, T_g and γ are kept fixed at the values $T_g = 80.00$ K and $\gamma = 1.80$, obtained from the ROF analysis, and the exponent β is varied so that the $\chi_{\rm nl}$ data at different but fixed static fields collapse onto a single universal $\chi_{\rm nl}/\epsilon^{\beta}$ versus $H^2/\epsilon^{\beta+\gamma}$ scaling plot. The residual freedom, if any, in T_g, β, and γ is then used to obtain the best data collapse over the largest possible range of the scaling argument, which corresponds to the ϵ range 1.1×10^{-3}–1.3×10^{-1}. Figure 4 demonstrates that a very good data collapse is achieved for the choice $T_g = 80.00(8)$ K, $\beta = 0.56(4)$, and $\gamma = 1.80(5)$. Note that the $\chi_{\rm nl}$ data used to construct the scaling plot are obtained by subtracting $\chi_1(T, h = 1$ Oe$, \omega = 100$ Hz), for fixed H, from the FC $\chi_{dc}(T, H = 10$ Oe). But for a slight increase in the scatter in the scaling plot, results similar to those presented in Fig. 4 are obtained when $\chi_1(T, h = 0.1$ Oe$, \omega = 10$ Hz) data are used.

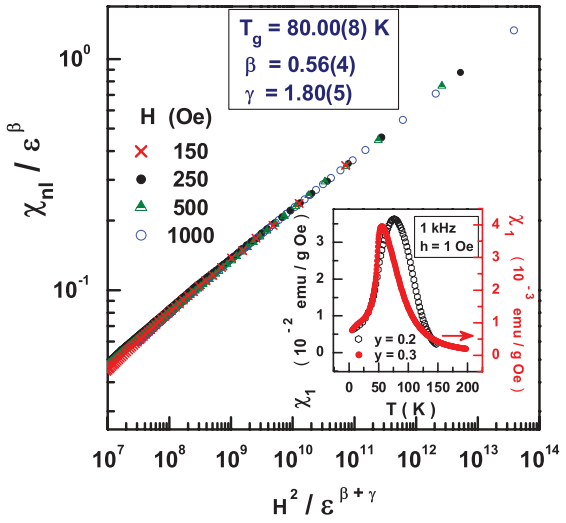

FIG. 4. (Color online) The reduced nonlinear susceptibility $\chi_{\rm nl}/\epsilon^{\beta}$ plotted against the reduced conjugate static field $H^2/\epsilon^{\beta+\gamma}$ for the composition $y = 0.2$. The validity of the static scaling Eq. (3) is demonstrated by an optimum collapse of the data, taken at different static fields, onto a single universal scaling curve for the choice $T_g = 80.00(8)$ K, $\beta = 0.56(4)$, and $\gamma = 1.80(5)$. The inset compares the linear susceptibilities of the samples $y = 0.2$ and $y = 0.3$, measured, in the absence of static field, at the ac field amplitude of $h = 1$ Oe and frequency $\omega = 1$ kHz.

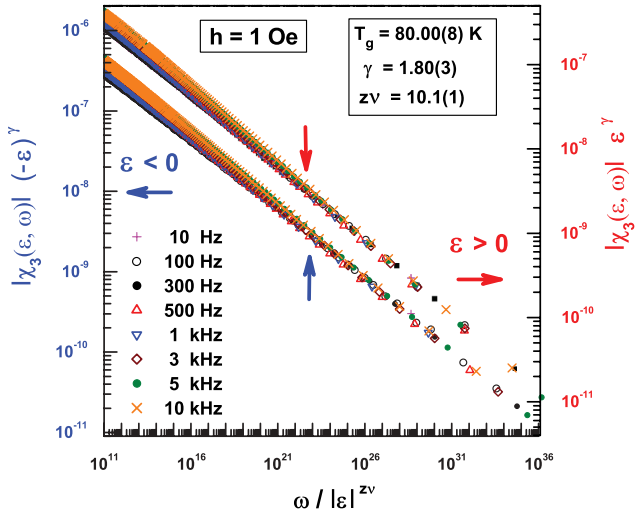

FIG. 5. (Color online) Dynamic scaling of the nonlinear susceptibility χ_3, based on Eq. (4) of the text, for temperatures below ($\epsilon < 0$) and above ($\epsilon > 0$) T_g. Vertical arrows mark the bifurcation temperatures (see text).

Similarly, at first, we set $T_g = 80.00$ K, $\gamma = 1.80$, and $\beta = 0.56$ and vary the exponent $z\nu$ in the dynamic scaling plots for $\chi_3(\epsilon,\omega)$ and $\chi_5(\epsilon,\omega)$, based on Eq. (4), to accomplish a good data collapse separately for temperatures below ($\epsilon < 0$) and above ($\epsilon > 0$) T_g. In the next step, the parameters T_g, β, γ, and $z\nu$ are fine tuned to optimize the data collapse over as large a range of $\omega/|\epsilon|^{z\nu}$ as possible while aiming at achieving the best data collapse in the vicinity of $\epsilon = 0$. Since the quality of data collapse cannot be directly assessed from the scaling plots, presented in Figs. 5 and 6, because of the insensitive nature of logarithmic scales, a blow-up of these scaling plots over every decade of the scaling argument $\omega/|\epsilon|^{z\nu}$ reveals that, for the choice $T_g = 80.00(8)$ K, $\gamma = 1.80(3)$, $\beta = 0.56(3)$, and $z\nu = 10.1(2)$, the SG dynamic scaling, Eq. (4), holds (scatter <5%) in the range $10^8 \leqslant \omega/|\epsilon|^{z\nu} \leqslant 3.7 \times 10^{33}$ for $\epsilon > 0$ and $10^{10} \leqslant \omega/|\epsilon|^{z\nu} \leqslant 3.7 \times 10^{33}$ for $\epsilon < 0$ over three decades of frequency $10^1 \leqslant \omega \leqslant 10^4$ Hz. These ranges of the scaling argument correspond to the reduced temperature ranges $1.0 \times 10^{-3} \leqslant \epsilon \leqslant 2.3 \times 10^{-1}$ and $1.0 \times 10^{-3} \leqslant (-\epsilon) \leqslant 1.3 \times 10^{-1}$, respectively. While the $\chi_3(\epsilon,\omega)$ and $\chi_5(\epsilon,\omega)$ data for the frequencies 3, 5, and 10 kHz, like those taken at frequencies $\omega \leqslant 1$ kHz, obey dynamic scaling in the above temperature ranges below and above T_g, the former set of data starts deviating from the latter set at $\epsilon = -1.05 \times 10^{-2}$ for $\epsilon < 0$ and $\epsilon = 1.25 \times 10^{-2}$ for $\epsilon > 0$. The bifurcation in the two sets of data is all the more pronounced in the scaling plots for $\chi_5(\epsilon,\omega)$ in Fig. 6. Although higher values of $z\nu$, β, and/or γ get rid of this bifurcation, they spoil the agreement between the two sets of data at temperatures close to T_g where the dynamic scaling should be valid at all frequencies if the SG transition at T_g is a thermodynamic phase transition. Since the dynamic spin-spin correlation length is related to the frequency as $\omega \propto \xi^{-z}$, the contribution to $\chi_3(\epsilon,\omega)$, and more so to $\chi_5(\epsilon,\omega)$, from the FM clusters becomes important when the frequency exceeds a threshold value, because at such frequencies ξ becomes comparable to the sizes of such clusters. Another important point to note is that the deviations from the dynamic scaling are observed when the temperature approaches T_g more closely than $\epsilon = 1.0 \times 10^{-3}$ or when the temperature falls outside the ACR on either side of T_g. While the deviations as $\epsilon \to 0$ could be a consequence of the well-known fact that the waiting time of 30 min is not sufficient for the spin system to attain complete thermodynamic equilibrium, those outside the ACR may reflect either the increasing importance of the "correction-to-scaling" terms or magnetic aging, particularly for $T \ll T_g$ (the SG aging effects become apparent at temperatures below $T \simeq 0.8T_g$). At this stage, it should be emphasized that the present manganite system marks the only spin-glass system for which the dynamic scaling of $\chi_5(\epsilon,\omega)$ has been demonstrated so far and T_g could be approached as closely as $\epsilon = 1.0 \times 10^{-3}$.

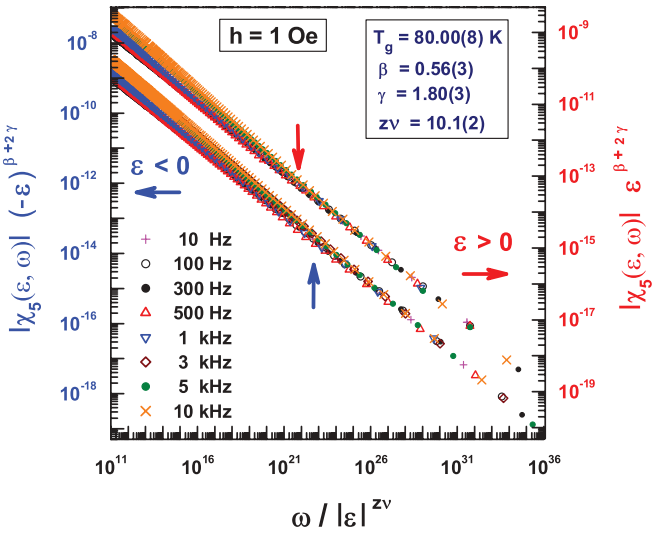

FIG. 6. (Color online) Dynamic scaling of the nonlinear susceptibility χ_5, based on Eq. (4) of the text, for temperatures below ($\epsilon < 0$) and above ($\epsilon > 0$) T_g. Vertical arrows mark the bifurcation temperatures (see text).

C. Dynamic scaling of $\chi_1''(\omega, T)$

For an independent determination of the exponents $z\nu$ and β, we use the dynamic scaling equation for $\chi_1''(\omega, T)$, proposed by Geschwind *et al.*,[24]

$$T\chi_1''(\omega,T)/\epsilon^{\beta} = g_1(\omega/\epsilon^{z\nu}). \quad (6)$$

Setting $T_g = 80.0$ K and varying β and $z\nu$, a nearly perfect data collapse (scatter <4%), as witnessed in Fig. 7, is obtained for the $\chi_1''(\omega,T)$ data taken over three decades of frequency in the reduced temperature range $-0.13 \leqslant \epsilon \leqslant \epsilon_{co}(\omega)$ [where $\epsilon_{co}(\omega)$ decreases from 0.27 at $\omega = 10^1$ Hz to 0.23 at $\omega = 10^4$ Hz] for the choice $\beta = 0.56(2)$ and $z\nu = 9.9(5)$. These values for β and $z\nu$ as well as the temperature ranges over which the dynamic scaling of $\chi_1''(\omega,T)$ holds are in excellent agreement with those determined earlier from the static and dynamic scaling of the NL susceptibilities. Consistent with the observations made based on the dynamic scaling of $\chi_3(\epsilon,\omega)$ and $\chi_5(\epsilon,\omega)$, the quality of data collapse deteriorates greatly when $\epsilon > \epsilon_{co}(\omega)$.

In order to ensure that departures from perfect scaling, Eq. (6), that are considerably larger than the experimental error

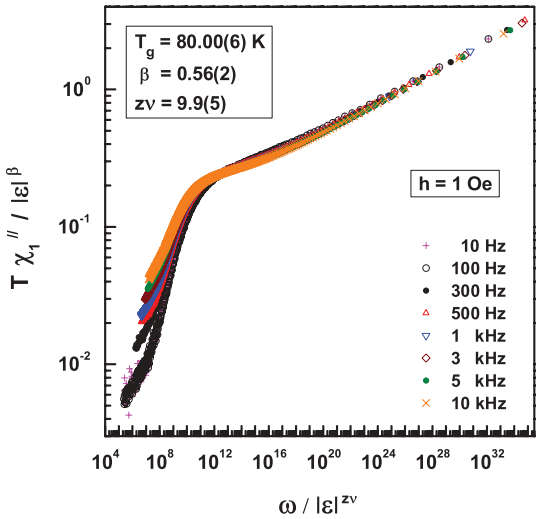

FIG. 7. (Color online) Dynamic scaling of the imaginary part of the linear susceptibility $\chi_1''(T)$ based on Eq. (6).

are not concealed by the $\log_{10}$-$\log_{10}$ plot in Fig. 7, the data used in Fig. 7, with exactly the same parameter values $T_g = 80.00(6)$ K, $\beta = 0.56(2)$, and $z\nu = 9.9(5)$ as those obtained using Eq. (6), are replotted according to the alternative form of the dynamic scaling equation,[24]

$$T\chi_1''(\omega,T)/\omega^{\beta/z\nu} = f_1(\epsilon/\omega^{1/z\nu}), \tag{7}$$

which is expected to bring out clearly any such departures due to the high sensitivity of the ordinate and abscissa scales. With the parameter values stated above, the same observations about the validity or otherwise of the dynamic scaling of $\chi_1''(\omega,T)$ are made regardless of whether the scaling equation (6) or (7) is used, as is evident from Fig. 8. However, the use of Eq. (7) clearly demonstrates that the overall scatter in the scaling plots within the temperature ranges where the

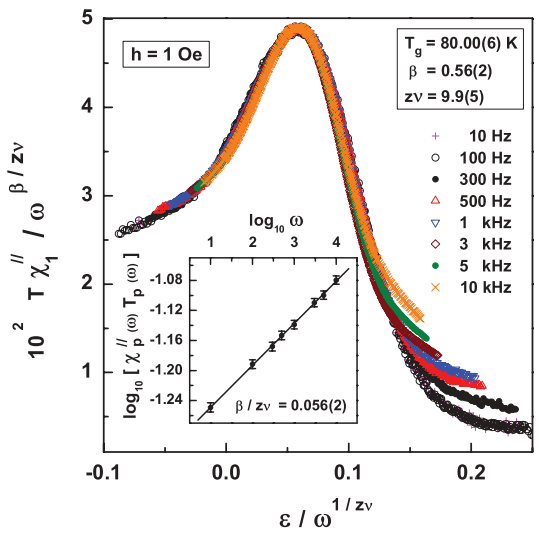

FIG. 8. (Color online) Dynamic scaling of the imaginary part of the linear susceptibility $\chi_1''(T)$ based on Eq. (7). The linear plot of $\log_{10}[\chi_p''(\omega)T_p(\omega)]$ against $\log_{10}\omega$ with slope $\beta/z\nu = 0.056(2)$ in the inset demonstrates the validity of the scaling relation $\chi_p''(\omega)T_p(\omega) \sim \omega^{\beta/z\nu}$.

$\chi_1''(\omega,T)$ data follow dynamic scaling over three decades of frequency does not exceed 3%, which is comparable to the typical scatter in the low-frequency ($\omega \leqslant 300$ Hz) data. The main advantage in employing Eq. (7) instead of Eq. (6) is that it provides an independent estimate of the ratio $\beta/z\nu$ as follows. According to Eq. (7), the peaks in $T\chi_1''(\omega,T)$ at $T_p(\omega)$, where $\chi_1''(\omega) = (\chi_1'')_p(\omega) \equiv \chi_p''(\omega)$, must collapse onto a single point on the scaling plot with the result that $\chi_p''(\omega)T_p(\omega) \sim \omega^{\beta/z\nu}$. The inset of Fig. 8 demonstrates that the plot of $\log_{10}[\chi_p''(\omega)T_p(\omega)]$ against $\log_{10}\omega$ is indeed a straight line with slope $\beta/z\nu = 0.056(2)$. This ratio conforms well with the values determined for β and $z\nu$ individually throughout this work from different forms of scaling, static or dynamic, and from the critical slowing down. Considering that a t_w of 15 min (30 min) amounts to $\sim 10^4\ \tau_{\chi''}$ ($\sim 2 \times 10^4\ \tau_{\chi''}$), where $\tau_{\chi''}$ is the characteristic time for χ_1'' at $\omega = 10$ Hz ($\tau_{\chi''} \sim 1/\omega$) for temperatures not very far from T_g (in the immediate vicinity of T_g), the spin system presumably attains equilibrium even for the lowest frequency $\omega = 10$ Hz.

D. Comparison with theory

The above self-consistent method of data analysis yields $T_g = 56.25(5)$ K, $\beta = 0.63(3)$, $\gamma = 2.0(1)$, and $z\nu = 8.0(5)$ for the composition $y = 0.3$. These values of β, γ, and $z\nu$, like those for $y = 0.2$, fall within the ranges $0.5 \leqslant \beta \leqslant 0.9$, $2 \leqslant \gamma \leqslant 4$, and $7 \leqslant z\nu \leqslant 11$, reported for a wide variety of spin-glass systems.[1,2,16,17,22,25–28] For a recent compilation of the experimental values of critical exponents for $d = 3$ Heisenberg spin-glass materials with weak anisotropy, we refer the reader to the recent review by Campbell and Petit.[29] In Table I, the presently determined values for the critical exponents are compared with the best theoretical estimates, yielded hitherto by Monte Carlo simulations, for $d = 3$ bimodal ($\pm J$) or Gaussian Heisenberg chiral spin glasses (HCSGs) with weak random magnetic anisotropy[6,7,30] and $d = 3$ bimodal or Gaussian Ising spin-glass (ISG) systems.[31,32] To put such a comparison between theory and experiment in a proper perspective, one has to recognize that the theory calculates the critical exponents ν and η and uses the scaling and hyperscaling relations $\beta = \nu(1+\eta)/2$, $\gamma = (2-\eta)\nu$, and $\delta = (d+2-\eta)/(d-2+\eta)$ to obtain the exponents β, γ, and δ whereas the experiments determine β, γ, and occasionally δ, and deduce ν and η via the hyperscaling relations $d\nu = 2\beta + \gamma$ and $\eta = 2 - d(\delta-1)/(\delta+1)$. We have used the scaling and hyperscaling relations $\delta = 1 + (\gamma/\beta)$ and $d\nu = 2\beta + \gamma$ with $d = 3$ and $\eta = 2 - (\gamma/\nu)$ to arrive at the values of δ, ν, and η displayed in Table I. With the exception of the exponent β, all the exponents for the samples $y = 0.2$ and $y = 0.3$ possess values that are *closer* to those predicted by the HCSG model. Apart from the widely different exponent values for the HCSG and ISG models, the main distinguishing feature is the opposite sign of the exponent η. In the present case, η has the same magnitude (within the uncertainty limits) and sign as predicted by the HCSG model. Consistent with this observation, the SG transition temperature T_g follows the $H^{2/3}$ [inset (d) of Fig. 1(b)] variation with the static field that the HCSG model (which considers a weak coupling between the chiral and spin degrees of freedom induced by magnetic anisotropy) yields for the chiral-glass transition at low fields in

TABLE I. Comparison of the critical exponents determined in this work for the manganite system $La_{0.7}Pb_{0.3}(Mn_{1-y}Fe_y)O_3$ ($y = 0.2, 0.3$) with those reported for the canonical spin glass AgMn and with the best theoretical estimates (currently available) for the bimodal ($\pm J$) Heisenberg chiral spin glass (HCSG), the Gaussian (G)HCSG, the $\pm J$ Ising spin glass (ISG), and the GISG.

Exponent	AgMn (Ref. 2)	$y = 0.2$	$y = 0.3$	$\pm J$ HCSG (Ref. 30)	GHCSG (Refs. 6,7)	$\pm J$ ISG (Ref. 31)	GISG (Ref. 32)
β	0.9(2)	0.56(3)	0.63(3)	1.2(7)	1.1(3)	0.77(5)	0.77(5)
γ	2.3(2)	1.80(5)	2.0(1)	1.5(4)	2.0(5)	5.8(4)	5.8(3)
δ	3.3(3)	4.2(3)	4.2(3)	2.3(4)	2.75(4)	8.6(1)	8.5(8)
η	0.23(32)	0.14(13)	0.2(2)	0.8(2)	0.6(2)	−0.375(10)	−0.37(5)
ν	1.30(15)	0.97(4)	1.1(1)	1.2(2)	1.4(2)	2.45(15)	2.44(9)
z	5.3(8)	10.4(10)	7.3(12)				

a $d = 3$ Heisenberg spin glass with weak random anisotropy.[7] Incidentally, the Edwards-Anderson mean-field model also predicts the $H^{2/3}$ power-law dependence of T_g (Ref. 33) along the Almeida-Thouless *irreversibility line* in the (T, H) plane for a $d = 3$ ISG but *no thermodynamic* spin-glass *phase transition in finite fields* occurs in ISGs.[34] In contradiction with the above agreement between our results and the predictions of the HCSG model, the SG order-parameter critical exponent β turns out to be a factor of 2 smaller in magnitude. Instead, the numerical estimate given by the ISG model for β is closer to the observed value. The coexistence of ferromagnetic short-range order with SG order for $T \leqslant T_g$ (Sec. III E) may have a direct bearing on this discrepancy in the value of β. Note that in view of the scaling identity $\delta = 1 + (\gamma/\beta)$, the lower value of β is basically responsible for the value of δ higher than that predicted by the HCSG model. The present results thus favor the thesis that the randomly Fe-substituted optimally hole-doped manganite $La_{0.7}Pb_{0.3}(Mn_{1-y}Fe_y)O_3$ ($y = 0.2, 0.3$) behaves as a $d = 3$ (localized-spin) Heisenberg spin glass with weak random magnetic anisotropy in the critical region and that the observed phase transition at T_g basically reflects the chiral-glass transition of the isotropic Heisenberg SG.[7]

E. Ferromagnetic short-range order

Had it not been for the presence of the characteristic experimental signatures of FM short-range order in the temperature variations of the NL susceptibilities χ_2 and χ_4, displayed in Fig. 9 for $y = 0.2$, the results presented so far would have strongly indicated that the manganite system in question is, at best, a spin glass. At this stage, it should be recalled that $\chi_2(T)$ and $\chi_4(T)$ are better suited for a clear-cut distinction between a SG and a ferromagnet than $\chi_3(T)$ and $\chi_5(T)$. This is so because the divergences in $\chi_3(T)$ and $\chi_5(T)$ at T_g in a SG and at T_c in a ferromagnet are not radically different unless the long-range FM order is fully developed. In comparison, $\chi_2(T)$ and $\chi_4(T)$ are *zero* at all temperatures including those close to T_g in an ideal or canonical SG whereas they are *negative* and *diverge* at T_c in a ferromagnet. Based on these considerations, the $\chi_2(T)$ and $\chi_4(T)$ data, presented in Fig. 9, provide direct evidence for the existence of two different time (and hence length) scales for the SG and FM order: the long-range (global) SG order and the short-range FM order observed at the experimental time scales $\tau_{\text{expt}} \gtrsim 1$ ms (in the static limit) and $\tau_{\text{expt}} \lesssim 10^{-4}$ s, respectively. The short-range nature of FM order is inferred from the considerably broad negative peaks centered at $T_c \simeq 80$ K that result when the spin-spin correlation length ξ does not diverge, but remains finite, at T_c. Obviously, at a shorter time scale (high frequencies), smaller FM clusters (regions with ferromagnetically ordered spins) essentially dictate the magnetic response whereas in the static limit $t \to \infty$, global cluster SG order at $T \leqslant T_g$ (brought about by the competing interactions between the finite FM clusters) governs the thermal behavior of NL susceptibilities. The existence of two distinct time (or length) scales for SG and short-range FM order (Fig. 9) also explains the strong departures observed from the SG critical slowing down in the inset (c) of Fig. 1(a) and from the SG dynamic scaling of nonlinear susceptibilities and linear susceptibility in Figs. 5–8 at frequencies $\omega \geqslant 3$ kHz. For the sample with $y = 0.3$, a

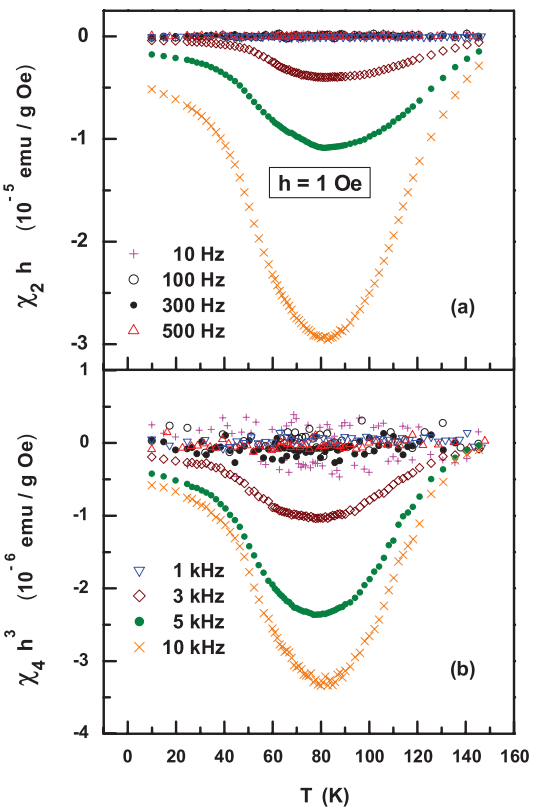

FIG. 9. (Color online) Temperature variations of the nonlinear susceptibilities χ_2 and χ_4 at different frequencies when $H = 0$ Oe and $h = 1$ Oe, revealing that the magnetic response is dominated by the long-range spin-glass order (short-range ferromagnetic order) at frequencies $\omega \leqslant 1$ kHz ($\omega \geqslant 3$ kHz).

broad negative peak centered at $T_c \simeq 56$ K in $\chi_2(T)$ and $\chi_4(T)$ first appears at $\omega = 10$ kHz, implying thereby that the FM order is prevalent over much shorter length scales than in the $y = 0.2$ sample. This inference is also supported by the observation that $\chi_1(T)$ is *lower by an order of magnitude* and exhibits a *much sharper* peak at $T_g \simeq 56$ K for $y = 0.3$ than for $y = 0.2$ (inset of Fig. 4). In conformity with this observation, the SANS data[13] corroborate that the FM-correlated regions shrink in size as the Fe concentration increases, such that the FM correlations do not grow beyond $\simeq 3$ nm in the $y = 0.2$ sample even at $T = T_c \simeq 80$ K, where $\xi(T)$ peaks. Note that for both samples with $y = 0.2$ and $y = 0.3$, T_g practically coincides with T_c, whereas the samples with lower Fe concentration (e.g., $y = 0.1$) exhibit two transitions: the high-temperature FM-PM transition followed, at much lower temperatures, by a reentrant transition.

IV. CONCLUDING REMARKS

The final picture that emerges from our results in the Fe concentration regime $0.2 \leqslant y \leqslant 0.3$ is the one in which completely isolated finite metallic FM clusters coexist with an infinite insulating SG (PM) matrix for $T \leqslant T_g$ ($T > T_g$). The double-exchange interactions between the spins of Mn^{3+} and Mn^{4+} nearest neighbors give rise to finite metallic FM clusters, whereas the insulating matrix is a consequence of the localization of e_g electrons on both Fe^{3+} and Mn^{3+} ions, because the high-spin states of Fe^{3+} and Mn^{3+} ions block the e_g-electron hopping[9] between them and also between Fe^{3+} and Fe^{3+} and between Mn^{3+} and Mn^{3+}. Random substitution of Mn^{3+} ions by Fe^{3+} ions and the competing FM and AFM interactions respectively cause the quenched random-exchange disorder and spin frustration that constitute the necessary ingredients for the cluster spin-glass state. The FM coupling between the magnetic moments of FM clusters is presumably due to the intercluster dipole-dipole interactions whereas the AFM coupling arises from the M_1^{3+}- O^{2-}- M_2^{3+} superexchange interactions, where M_1 and M_2 stand for either Fe or Mn. As elucidated in Ref. 23, the above percolation picture, applicable to all those hole-doped manganites with quenched random-exchange disorder that are below, but close to, the threshold for long-range FM or AFM order, is strikingly similar to the percolation model proposed earlier[35] for amorphous ferromagnets. According to this picture,[23,35] the crossover temperature ϵ_{co} above which $\gamma_{\rm eff}(\epsilon)$ in Fig. 3(b) starts increasing from the asymptotic value of $\gamma = 1.8$ corresponds to the temperature at which the SG spin-spin correlation length ξ equals the caliper dimension D_c of the largest FM spin cluster. Thus, an estimate of the size of FM clusters can be made from the relation $\xi(\epsilon = \epsilon_{co}) = D_c = r_{\rm av}\, \epsilon_{co}^{-\nu}$, where $r_{\rm av}$ is the average nearest-neighbor distance between the M_1^{3+} and M_2^{3+} ions. Inserting $r_{\rm av} = 0.3925$ nm (0.3928 nm),[9] $\epsilon_{co} = 0.25(2)$ [$\epsilon_{co} = 0.45(5)$], and $\nu = 0.97(4)$ [$\nu = 1.1(1)$] in the above relation yields an average FM spin cluster size of 2.0(5) nm [1.0(2) nm] for $y = 0.2$ [$y = 0.3$]. The average FM cluster size for $y = 0.2$, so determined, compares well with that deduced from the SANS data.[13] Furthermore, the considerably smaller value of the exponent β compared to that theoretically predicted for a $d = 3$ Heisenberg chiral spin glass with weak random magnetic anisotropy indicates that a meaningful comparison between theory and experiment is possible only when the probability of finding magnetic impurity atoms as nearest neighbors, in a nonmagnetic host, is extremely low or when the theory takes into account the influence of magnetic short-range order on the critical behavior of spin-glass systems. The existence of magnetic short-range order could also be a root cause for a wide dispersion in the exponent values reported for spin-glass systems.

At this stage, it should be mentioned that the nuclear magnetic resonance (NMR) technique has been widely used to detect FM clusters (the FM cluster spin-glass phase) in an AFM (PM) matrix in manganites[36–41] and AFM clusters constituting the cluster spin-glass phase that coexists with superconductivity in underdoped La-based cuprates.[42,43] Unlike nonlinear susceptibility, which provides a direct experimental evidence for both FM or AFM short-range order (clusters) and the spin-glass state, NMR indirectly infers the existence of a SG state through the appearance of the critical-slowing-down features in the temperature dependence of the nuclear-spin–lattice relaxation rate.

To summarize, a combined investigation of both odd and even harmonics of the ac magnetic response enables one to unambiguously distinguish between a canonical and a cluster spin glass. While the odd harmonics yield true asymptotic values of the critical exponents (that characterize the universality class of the spin-glass system in question), the even harmonics not only confirm the presence or absence of correlated-spin regions (spin clusters) but also reveal the nature of the intracluster magnetic order.

ACKNOWLEDGMENTS

This work was supported by the Department of Science and Technology, India, through Grant No. IR/S5/IU-01/2006, and by the Spanish Ministry for Education through the grant No. SAB 2010-0091. S.N.K. is thankful to the Department of Science and Technology, India, for financial support through the J. C. Bose National Fellowship. Y.B. thanks the Council for Scientific and Industrial Research, India, for the financial support through a Senior Research Fellowship. The authors thank J. M. Barandiarán and J. Gutiérrez for providing the samples.

*kaulsp@uohyd.ernet.in

[1] J. A. Mydosh, *Spin Glasses: An Experimental Introduction* (Taylor and Francis, London, 1993).
[2] L. P. Lévy and A. T. Ogielski, Phys. Rev. Lett. **57**, 3288 (1986); L. P. Lévy, Phys. Rev. B **38**, 4963 (1988).
[3] R. E. Walstedt and L. R. Walker, Phys. Rev. Lett. **47**, 1624 (1981); A. Chakrabarti and C. Dasgupta, *ibid.* **56**, 1404 (1986).
[4] L. W. Lee and A. P. Young, Phys. Rev. Lett. **90**, 227203 (2003); L. Berthier and A. P. Young, Phys. Rev. B **69**, 184423 (2004).
[5] L. A. Fernandez, V. Martin-Mayor, S. Perez-Gaviro, A. Tarancon, and A. P. Young, Phys. Rev. B **80**, 024422 (2009).
[6] D. X. Viet and H. Kawamura, Phys. Rev. B **80**, 064418 (2009).
[7] H. Kawamura, J. Phys. Soc. Jpn. **79**, 011007 (2010).

[8]E. Dagotto, *Nanoscale Phase Separation and Colossal Magnetoresistance* (Springer, Berlin, 2003).
[9]J. Gutiérrez, A. Peña, J. M. Barandiarán, J. L. Pizarro, T. Hernandez, L. Lezama, M. Insausti, and T. Rojo, Phys. Rev. B **61**, 9028 (2000).
[10]G. Gritzner, M. Koppe, K. Kellner, J. Przewoznik, J. Chmist, A. Kolodziejczyk, and K. Krop, Appl. Phys. A: Mater. Sci. Process. **81**, 1491 (2005).
[11]S. L. Young, H. Z. Chen, M. C. Kao, L. Horng, and Y. T. Shih, J. Magn. Magn. Mater. **303**, e351 (2006).
[12]J. Gutiérrez, F. J. Bermejo, J. M. Barandiarán, S. P. Cottrell, P. P. Romano, C. Mondelli, J. R. Stewart, L. Fernández Barquín, and A. Peña, Phys. Rev. B **73**, 054433 (2006).
[13]J. Gutiérrez, F. J. Bermejo, N. Veglio, J. M. Barandiarán, P. Romano, C. Mondelli, M. A. González, and A. P. Murani, J. Phys.: Condens. Matter **18**, 9951 (2006).
[14]J. Gutiérrez, J. M. Barandiarán, F. J. Bermejo, C. Mondelli, P. Romano, P. Fouquet, and M. Monkenbusch, Phys. Rev. B **76**, 184401 (2007).
[15]J. M. Barandiarán, F. J. Bermejo, J. Gutiérrez, and L. Fernández Barquín, J. Non-Cryst. Solids **353**, 757 (2007).
[16]A. Mauger, J. Ferré, M. Ayadi, and P. Nordblad, Phys. Rev. B **37**, 9022 (1988).
[17]G. F. Goya and V. Sagredo, Phys. Rev. B **64**, 235208 (2001).
[18]N. Bontemps, J. Rajchenbach, R. V. Chamberlin, and R. Orbach, Phys. Rev. B **30**, 6514 (1984).
[19]M. Suzuki, Prog. Theor. Phys. **58**, 1151 (1977); K. Wada and H. Takayama, *ibid*. **64**, 327 (1980); S. Fujiki and S. Katsura, *ibid*. **65**, 1130 (1981).
[20]Y. Bitla and S. N. Kaul, Europhys. Lett. **96**, 37012 (2011).
[21]J. Chalupa, Solid State Commun. **24**, 429 (1977).
[22]K. Gunnarsson, P. Svedlindh, P. Nordblad, L. Lundgren, H. Aruga, and A. Ito, Phys. Rev. B **43**, 8199 (1991).
[23]Y. Bitla, S. N. Kaul, L. Fernández Barquín, J. Gutiérrez, J. M. Barandiarán, and A. Peña, New J. Phys. **12**, 093039 (2010), and references cited therein.
[24]S. Geschwind, D. A. Huse, and G. E. Devlin, Phys. Rev. B **41**, 4854 (1990).
[25]A. Labarta, X. Batlle, B. Martínez, and X. Obradors, Phys. Rev. B **46**, 8994 (1992).
[26]B. Leclercq, C. Rigaux, A. Mycielski, and M. Menant, Phys. Rev. B **47**, 6169 (1993).
[27]R. Mathieu, A. Asamitsu, Y. Kaneko, J. P. He, and Y. Tokura, Phys. Rev. B **72**, 014436 (2005).
[28]S. Nair and A. K. Nigam, Phys. Rev. B **75**, 214415 (2007).
[29]I. A. Campbell and D. C. M. C. Petit, J. Phys. Soc. Jpn. **79**, 011006 (2010).
[30]K. Hukushima and H. Kawamura, Phys. Rev. B **72**, 144416 (2005).
[31]M. Hasenbusch, A. Pelissetto, and E. Vicari, Phys. Rev. B **78**, 214205 (2008).
[32]H. G. Katzgraber, M. Körner, and A. P. Young, Phys. Rev. B **73**, 224432 (2006).
[33]J. R. L. de Almeida and D. J. Thouless, J. Phys. A **11**, 983 (1978).
[34]J. Mattsson, T. Jonsson, P. Nordblad, H. Aruga Katori, and A. Ito, Phys. Rev. Lett. **74**, 4305 (1995).
[35]S. N. Kaul, J. Magn. Magn. Mater. **53**, 5 (1985).
[36]G. Papavassiliou, M. Pissas, M. Belesi, M. Fardis, J. Dolinsek, C. Dimitropoulos, and J. P. Ansermet, Phys. Rev. Lett. **91**, 147205 (2003).
[37]Y. Kawasaki, T. Minami, Y. Kishimoto, T. Ohno, K. Zenmyo, H. Kubo, T. Nakajima, and Y. Ueda, Phys. Rev. Lett. **96**, 037202 (2006), and references cited therein.
[38]G. Papavassiliou, M. Pissas, G. Diamantopoulos, M. Belesi, M. Fardis, D. Stamopoulos, A. G. Kontos, M. Hennion, J. Dolinsek, J. P. Ansermet, and C. Dimitropoulos, Phys. Rev. Lett. **96**, 097201 (2006), and references cited therein.
[39]K. Shimizu, Y. Qin, and T. A. Tyson, Phys. Rev. B **73**, 174420 (2006).
[40]V. M. Vladimir, Y. Eero, S. Z. Vasilii, and L. Reino, J. Phys.: Condens. Matter **19**, 226209 (2007).
[41]N. Panopoulos, D. Koumoulis, G. Diamantopoulos, M. Belesi, M. Fardis, M. Pissas, and G. Papavassiliou, Phys. Rev. B **82**, 235102 (2010), and references cited therein.
[42]M.-H. Julien, F. Borsa, P. Carretta, M. Horvatić, C. Berthier, and C. T. Lin, Phys. Rev. Lett. **83**, 604 (1999).
[43]M.-H. Julien, A. Campana, A. Rigamonti, P. Carretta, F. Borsa, P. Kuhns, A. P. Reyes, W. G. Moulton, M. Horvatić, C. Berthier, A. Vietkin, and A. Revcolevschi, Phys. Rev. B **63**, 144508 (2001).